

# Equivalence classes of Fibonacci lattices and their similarity properties

N. Lo Gullo,<sup>1,2</sup> L. Vittadello,<sup>1</sup> M. Bazzan,<sup>1,2</sup> and L. Dell'Anna<sup>1,2</sup>

<sup>1</sup>*Dipartimento di Fisica e Astronomia, Università degli Studi di Padova, Padova, Italy*

<sup>2</sup>*CNISM, sezione di Padova*

(Dated: July 28, 2016)

We investigate, theoretically and experimentally, the properties of Fibonacci lattices with arbitrary spacings. Differently from periodic structures, the reciprocal lattice and the dynamical properties of Fibonacci lattices depend strongly on the lengths of their lattice parameters, even if the sequence of long and short segment, the Fibonacci string, is the same. In this work we show that, by exploiting a self-similarity property of Fibonacci strings under a suitable composition rule, it is possible to define equivalence classes of Fibonacci lattices. We show that the diffraction patterns generated by Fibonacci lattices belonging to the same equivalence class can be rescaled to a common pattern of strong diffraction peaks thus giving to this classification a precise meaning. Furthermore we show that, through the gap labeling theorem, gaps in the energy spectra of Fibonacci crystals belonging to the same class can be labeled by the same momenta (up to a proper rescaling) and that the larger gaps correspond to the strong peaks of the diffraction spectra. This observation makes the definition of equivalence classes meaningful also for the spectral, and therefore dynamical and thermodynamical properties of quasicrystals. Our results apply to the more general class of quasiperiodic lattices for which similarity under a suitable deflation rule is in order.

PACS numbers:

## I. INTRODUCTION

Since the first experimental proof of the existence of solids lacking of translational invariance, but exhibiting a discrete Bragg diffraction spectrum [1], the study of *quasicrystals* attracted quite a lot of attention. The impact of this discovery on the scientific community was such that in 1992 the former definition of crystal had to be modified in order to include those structures whose diffraction pattern witnesses long range order yet lacking translational invariance [2–4]. More generally, the study of quasiperiodic geometries has been recently the subject of different fields all devoted to the propagation of waves through quasiperiodic potentials. The spectral properties of quasicrystals have been recently used to engineer topological pumping in optical waveguides [5–7] and in ultracold gases [8, 9]. Engineering of quasiperiodic structures have also been employed in optical dielectric multilayers for resonant transmission [10], solar energy harvesting [11], plasmonics [12, 13] and nonlinear optics [14, 15].

Dynamical and transport phenomena in this kind of structures are also radically different compared to periodic media [16–20]. For usual periodic arrangements, dynamical and thermodynamical properties are directly related, via the Bloch theorem, to the geometry of the system. Quasiperiodic geometries, instead, lacks of translational invariance so that a direct relation between their structure and their dynamical properties is not generally known. It would be therefore very interesting to find a sort of classification enabling one to group together different aperiodic systems on the basis of some similarity between their geometric arrangements. In this paper we attempt to define such a classification, showing that quasiperiodic structures whose geometry is related by a suitable mathematical transformation share the main characteristics of their reciprocal lattice and of their pseudo-band structure.

## II. GENERALIZED FIBONACCI LATTICES

In one dimension (1D) the paradigm of a quasicrystal is the Fibonacci lattice (FL). The FL is a 1D lattice whose adjacent points have distances belonging to the set  $\{L, S\}$ , standing for Long and Short respectively, which are arranged according to a given sequence. Such a lattice can be constructed by means of the cut and project technique [3, 4, 21] thus obtaining for the coordinates of points on the real line [2] (in units of  $S$ ):

$$x_n^\eta = n - 1 + \frac{1}{\eta} \left\lfloor \frac{n}{\tau} \right\rfloor \quad (1)$$

where  $n$  is a natural positive number,  $\lfloor x \rfloor$  is the integer part of  $x$  and  $\eta = S/(L - S)$ . The most common instance found in literature is obtained for  $\eta = \tau = (\sqrt{5} + 1)/2$ , the golden ratio. In this case the canonical FL (CFL) is obtained, such that the lengths are (up to a simple rescaling):  $L = 1 + 1/\tau = \tau$ , and  $S = 1$ . Nevertheless it is possible to construct Fibonacci lattices with  $\eta \neq \tau$  (see App. A). The distances  $\Delta_n = x_{n+1}^\eta - x_n^\eta$  are either  $L = 1 + 1/\eta$  or  $S = 1$  and they are arranged according to the Fibonacci string (FS)  $LSLLSLSLLSLLSLSLLSLSL \dots$ . The latter is any word made of two letters,  $L$  and  $S$ , obtained by means of the substitution rule  $S \rightarrow L$  and  $L \rightarrow LS$  starting from the letter  $L$ . We notice that a FS itself is independent on the parameter  $\eta$  and it only depends on the factor  $1/\tau$ .

Conversely, given an infinite FS, a composition rule ( $LS \rightarrow L'$  and  $L \rightarrow S'$ ) can be defined such that the old and the new strings are the same due to the peculiar properties of the Fibonacci strings, as shown in Fig. 1. For the special case  $\eta = \tau^k$ , with  $k$  a non-vanishing integer i.e. for the canonical FL, this leads to a peculiar property: the new FL can be rescaled to the original one. This case is the most commonly encountered in literature, accompanied by the statement that the CFL is *self-similar*. It should be stressed however that this is not true for the general case  $\eta \neq \tau^k$ . In this case, a

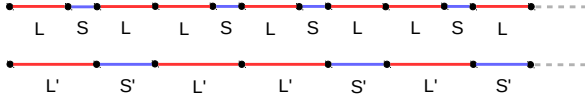


Figure 1: The composition rules ( $LS \rightarrow L'$ ,  $L \rightarrow S'$ ) on a semi-infinite Fibonacci lattice reproduces another Fibonacci lattice with different lattice parameters.

non-canonical Fibonacci lattice and the one obtained by applying the composition rule are characterized by two different length ratios  $\eta_1$  and  $\eta_2$  because  $L'/L \neq S'/S$ . Therefore the new lattice cannot be transformed into the old one by a simple rescaling.

We call  $\mathcal{C}$  the operator corresponding to the effect of the composition rule on the FL  $x_n^\eta$ . It is not difficult to show that  $\mathcal{C}(x_n^\eta) = \eta_1 x_n^{\eta_1}$ , where  $\eta_1 = 1 + 1/\eta$ : the composition rule maps a FL  $x_n^\eta$  into another FL, characterized by a new ratio  $\eta_1$  and rescaled by  $\eta_1$  (see Fig. 1). If  $\eta = \tau$  then  $\eta_1 = \tau$  (recall that  $\tau^2 - \tau - 1 = 0$ ) and therefore the CFL is self-similar. If the composition rule is applied  $k$  times, the initial FL is mapped into

$$\mathcal{C}^{(k)}(x_n^\eta) = \left( \prod_{i=1}^k \eta_i \right) x_n^{\eta_k} = \left( F_{k+1} + \frac{F_k}{\eta} \right) x_n^{\eta_k} \quad (2)$$

where  $\eta_i = 1 + 1/\eta_{i-1}$  ( $\eta_0 = \eta$ ) and  $F_k$  are the Fibonacci numbers. With the help of this concept we define equivalence classes for FLs by means of the following equivalence relation:

**Definition -** Two Fibonacci lattices  $x_n^{\eta_a}$  and  $x_n^{\eta_b}$  are equivalent ( $x_n^{\eta_a} \sim x_n^{\eta_b}$ ) if they are linked, up to a proper rescaling, by means of the composition rule  $\mathcal{C}$ . The lattice with the minimum  $\eta_0$  such that  $1/(\eta_0 - 1)$  is finite and positive is called the generator of the equivalence class which is denoted by  $[\eta_0]$ .

A simple way of labeling the elements of a given equivalence class is by means of the continued fraction representation for the  $\{\eta_i\}$ .

Because of this, for quasiperiodic structures it is of limited practical utility to talk about the support of the diffraction pattern. It is more meaningful to describe the diffraction spectrum (and the reciprocal lattice) in terms of the peaks which are significantly close to one, which will be referred to as brightest peaks. By means of the cut and project method outlined in App. A it is possible to show (see App. B) that the intensity  $I(q, \eta)$  at points  $q = Q(h, h')$  is given by  $\text{sinc}^2(Q_\perp(h, h')\Delta)$ , where  $Q_\perp(h, h') = 2\pi d^{-1}(h(1 + 1/\eta)^{-1} - h')$  and  $\Delta = \tau(\eta/(\eta + 1))/2$ . Therefore the brightest peaks are found for pairs  $(h, h')$  such that  $Q_\perp(h, h') \approx 0$  and thus for

$$\frac{h}{h'} = 1 + \frac{1}{\eta}. \quad (3)$$

Since  $h$  and  $h'$  are integers, the above condition can be satisfied exactly only if  $\eta$  is a rational number. On the other hand

for irrational  $\eta$  we can resort to its continued fraction representation in order to set the wanted precision to the above condition.

Let us now consider two FLs belonging to the same equivalence class  $x_n^{\eta_0}$  and  $x_n^{\eta_1}$ , with  $\eta_1 = 1 + 1/\eta_0$ . By defining  $h_n(k_n)$  and  $h'_n(k'_n)$  as the numerator and denominator of the  $n$ -th rational approximants of  $1 + 1/\eta_0$  ( $1 + 1/\eta_1$ ), the following relations hold:  $k_n = h_n + h'_n$  and  $k'_n = h_n$ . The position of the brightest peaks of the FL  $x_n^{\eta_1}$  are then related to those of the FL  $x_n^{\eta_0}$  by:

$$Q_1(k_n, k'_n) = \eta_1 Q_0(h_n, h'_n) \quad (4)$$

In other words, although the two Fibonacci lattices  $x_n^{\eta_0}$  and  $\mathcal{C}(x_n^{\eta_0}) = \eta_1 x_n^{\eta_1}$  cannot be rescaled one over the other (for the general case  $\eta \neq \tau$ ), their brightest peak pattern can, as a consequence of the fact that they are related by the composition rule. Also the intensities of the brightest peaks can be related as  $I(\eta_1 q, \eta_1) \approx I(q, \eta_0) + \frac{1}{\tau}(1 - I(q, \eta_0))$  (for  $q$  such that  $I(q, \eta_0) > 0.5$ ) showing that the peaks of the scaled lattice are even brighter than those of the original lattice. This drives to the important conclusion that FL belonging to the same equivalence class have diffraction spectra characterized by the same pattern of brightest peaks, and are, in this sense, similar.

### III. SIMILARITY OF DIFFRACTION PATTERNS

To quantify the degree of similarity between the two spectra, we use the Kullback-Leibler divergence (KLD), a quantity useful to compare two distributions (normalized to unity over a common support). Let us consider the diffraction spectra  $I(q, \eta_\alpha)$  and  $I(q, \eta_\beta)$  of two arbitrary FL's characterized by  $\eta_\alpha \neq \eta_\beta$ . We define the normalized spectrum:  $P(\nu q, \eta) = I(\nu q, \eta) / \int_0^\infty dk I(\nu k, \eta)$  where we introduced a scaling parameter  $\nu$ .

The KLD is defined as:

$$D(\eta_\alpha, \eta_\beta, \nu) = \int_0^\infty dk P(k, \eta_\alpha) \log \left( \frac{P(k, \eta_\alpha)}{P(\nu k, \eta_\beta)} \right). \quad (5)$$

By definition one has that the more similar the two diffraction spectra, the smaller the value of the KLD. We will use it to measure if, for given  $\eta_\alpha$  and  $\eta_\beta$ , there exist a scaling parameter  $\nu$  for which the two spectra look similar.

In Fig. 2 a) and b) we plot  $1/D(\eta_0^\alpha, \eta, \nu)$  comparing two generators corresponding to  $\eta_0^a = 6/11$  and  $\eta_0^b = 1/6$  with FLs obtained from them by applying the composition rule  $\mathcal{C}^{(n_\alpha)}$  respectively  $n_a = 1$  and  $n_b = 3$  times. The intensities  $I(q, \eta)$  are evaluated by means of eq.B15 for lattices with  $N = 300$  points. The maxima (minima of  $D$ ) in the two figures correspond to  $(\eta, \nu) = (\eta_1^a, \eta_1^a)$  and  $(\eta, \nu) = (\eta_1^b, \eta_1^b \eta_2^b \eta_3^b)$  respectively, in agreement with eq. (4). This shows that two FL's produce a similar diffraction pattern if and only if they can be related via Eq. (2) and therefore only if they belong to the same equivalence class.

In order to test our results on a real case, we performed a diffraction experiment on two quasiperiodic diffraction gratings prepared using a photorefractive direct laser writing

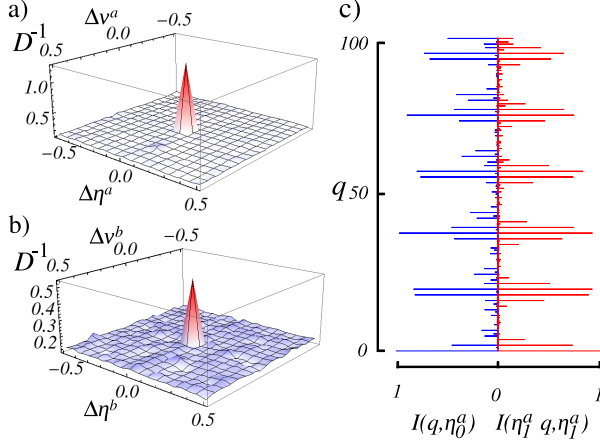


Figure 2: (Color online) Inverse of KL divergence  $1/D(\eta_0^a, \eta, \nu)$  comparing the diffraction spectra of the generator of a given class  $x_n^{\eta_0}$  with another Fibonacci lattice, for two choices of  $\eta_0$ . a)  $\eta_0^a = 6/11$ ; b)  $\eta_0^b = 1/6$ . Here  $\Delta\eta^a = \eta - \eta_1^a$ ,  $\Delta\nu^a = \nu - \eta_1^a$  and  $\Delta\eta^b = \eta - \eta_1^b$ ,  $\Delta\nu^b = \nu - \eta_1^b \eta_2^b \eta_3^b$ . The maxima (minima of  $D(\eta_\alpha, \eta_\beta, \nu)$ ) are obtained at  $\Delta\eta^{a,b} = 0$  and  $\Delta\nu^{a,b} = 0$ , indicating that the two spectra with the highest degree of similarity corresponds to lattices  $\eta_1^a x_n^{\eta_1^a} = C(x_n^{\eta_0^a})$  and  $\eta_1^b \eta_2^b \eta_3^b x_n^{\eta_3^b} = C^{(3)}(x_n^{\eta_0^b})$  respectively, i.e. the first and the third element of the respective equivalence classes. c) Direct comparison of the two diffraction spectra for two FLs  $x_n^{\eta_0^a}$  and  $\eta_1^a x_n^{\eta_1^a}$ . The most prominent peaks of the diffraction pattern  $I(q, \eta_0^a)$  correspond with those of the (rescaled) spectrum  $I(\eta_1^a q, \eta_1^a)$ .

(DLW) technique [25, 26]. We used three gratings made up of  $N = 300$  lines all written in the same substrate: (a) a periodic grating with spacing  $L = 23\mu\text{m}$ ; two Fibonacci gratings with (b)  $L = 23\mu\text{m}$  and  $S = 17\mu\text{m}$  ( $\eta_1^a = 17/6$ ) and (c)  $L = 23\mu\text{m}$  and  $S = 15\mu\text{m}$  ( $\eta_3^b = 15/8$ ) respectively. So far we considered point lattices, but real structures are constituted by some physical entity (basis) arranged on the points of our quasi-periodic Fibonacci lattice. (For a detailed description of the experimental set up see App. E). For these cases, the diffraction pattern is given by the sum in Eq. (B15) multiplied by the square modulus of a structure factor. The latter, in general, does not possess any scaling property and therefore it is necessary to correct for it when comparing different lattices. We did this experimentally by using the data of the periodic grating to extract a phenomenological expression for the structure factor as a function of  $q$ . In Fig. 3 a) we compare the experimental data relative to the grating  $\eta_1^b$  with the theoretical diffraction pattern obtained from the generator of the corresponding equivalence class,  $\eta_0^b = 1/6$ . We observe that, once the spectra have been rescaled in  $q$  following eq. (4) and corrected in order to take into account the structure factor contribution to the intensity of the peaks, the most prominent diffraction features of the generator can be found in the experimental data at the correct  $q$  positions. The degree of similarity between the spectrum of the generator and the experimental one is confirmed by the KL divergence  $D$  between the experimental data points and the theoretical diffraction spectrum (with the inclusion of the structure factor) calculated for

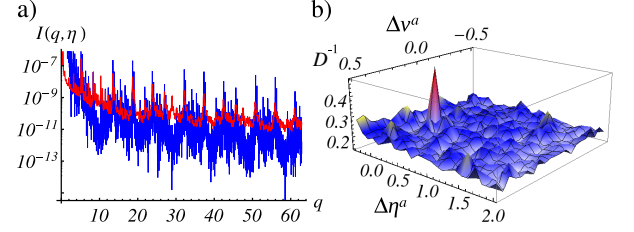


Figure 3: (Color online). a) Comparison between the theoretical diffraction pattern for the FL  $x_n^{\eta_0^a}$  ( $\eta_0^a = 0.5454$ , solid blue curve) and the experimental one produced by a FL  $C(x_n^{\eta_0^a})$  (solid red curve,  $N = 300$  lines and  $L = 23\mu\text{m}$  and  $S = 17\mu\text{m}$ ,  $\eta_1^a = 2.8\bar{3}$ ). The theoretical spectrum has been rescaled in accordance with Eq. (4) and corrected for the structure factor contribution. b) The inverse of KL divergence ( $D^{-1}(\eta_1^a, \eta, \nu)$ ) between the (normalized over the interval) experimental diffraction pattern and the theoretical diffraction patterns for different generators and different scaling. Here  $\Delta\eta^a = \eta - \eta_0^a$  and  $\Delta\nu = \nu - 1/\eta_0^a$ . The maximum (minima of  $D$ ) is at  $(\eta, \nu) = (\eta_0^a, 1/\eta_0^a)$ .

a range of  $\eta_0$  and scaling factor  $\nu$ . In Fig. 3 b) we show it explicitly for the grating with  $\eta_1^a$  and it is clear that the maximum of  $D^{-1}$  (minimum of  $D$ ) is found at  $\eta_0 = \eta_0^a$  and  $\nu = \eta_1^{-1}$ . Similar results are obtained for the grating  $\eta_1^b$ .

#### IV. ENERGY SPECTRA COMPARISON

We have therefore shown that all the FL belonging to the same equivalence class have diffraction spectra that, although not equals, are characterized by a similar pattern of bright peaks. This finding is of crucial importance not only in scattering phenomena but also in transport ones. In fact in a recent work [23] a method to unambiguously link the gaps in the integrated density of states to the brightest peaks in the diffraction pattern of the underlying potential has been proposed. This is more general as it has been shown in a seminal paper by Luck [22]. Let us consider for example the Hamiltonian for a particle in a 1D lattice:

$$\hat{H} = -\frac{\hbar^2}{2} \frac{d^2}{dx^2} + V(x) \quad (6)$$

$$V(x) = -V_0 \int dy f(x-y) \sum_n \delta(y-x_n) \quad (7)$$

where  $x_n$  are the local minima of the potential and  $f(x)$  is introduced to account for the detailed shape of the potential minima ( $V_0 > 0$ ). We will consider the case  $x_n = x_n^\eta$  according to the quasi-periodic sequence of Eq. 1. In Ref. [23] it has been shown that it is possible to label the energy gaps by means of the brightest peaks of the diffraction spectrum. In particular one has to consider the pseudo-momenta  $q$  at which the square of the Fourier transform of  $V(x)$  acquires values greater than a given threshold. This effectively corresponds to choose which free states are effectively coupled by the potential and, therefore, where wider gaps open in the single

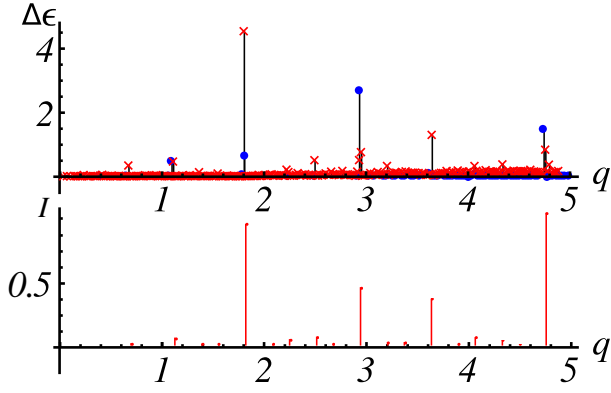


Figure 4: (Color online). Plot of the energy level spacings of the Hamiltonian in Eq.(7) for a potential  $V(x)$  having minima at the points of FLs  $x_n^\eta$  with (blue dots)  $\eta = \eta_0^a$ , (red crosses)  $\eta_1^a$ . Below we compare the gaps with the brightest peaks of  $I(q/\eta_1^a, \eta_1^a)$ .

particle spectrum. One of the results presented in Ref. [23] is that this is equivalent to set a threshold to the intensity of the peaks in the Bragg spectrum of the lattice. This can be easily seen by considering the Fourier transform of the potential  $V(x)$ , namely  $V(q) = \int e^{ixq} V(x) dx$  whose square modulus is given by:

$$|V(q)|^2 = S(q)I(q, \eta) \quad (8)$$

where  $S(q)$  is the square of the Fourier transform of  $f(x)$  and  $I(q, \eta)$  is given by Eq. B15. It is clear from what shown above and confirmed by the experiment on the diffraction patterns, that, apart from the contribution of the actual form of the potential (which plays a role analogous to the structure factor in diffraction experiments), the energy pseudo-band structure in reciprocal space has the same shape (up to a rescaling) for the lattices belonging to a given class. As an example, we computed the spectra of Eq. (7) in the case of Gaussian wells, namely  $f(x) = e^{-x^2/2\sigma^2}$  for a system with  $N = 100$  minima and  $x_n = x_n^\eta$  with  $\eta = \eta_0^a, \eta_1^a$  and  $\eta = \eta_0^b, \eta_3^b$ . We choose  $V_0 = 12$ ,  $\sigma = 0.1$ . In Fig. 4 we plot the energy level spacing for lattices characterized by  $\eta_0^a = 6/11$  (blue dots) and  $\eta_1^a = 17/6$  (red crosses) both belonging to the equivalence class  $[\eta_0^a]$ . The momenta on the  $x$ -axis serve as a reference with respect to the free particle dispersion relation ( $\epsilon_k = k^2/2$ ,  $V(x) = 0$ ) to show where the potential  $V(x)$  opens the gaps. After rescaling the momenta for the lattices with  $\eta = \eta_1^a$  by  $\nu_a = \eta_1^a$  we can clearly see that the gaps appear at the same points. On the other hand these points correspond to the brightest peaks, where  $I(q/\eta_1^a, \eta_1^a)$  calculated by Eq. (B15) is sizeable. Similar results are obtained (not shown) for the equivalence class  $[\eta_0^b]$  with  $\eta_0^b = 1/6$  by considering the two lattices characterized by  $\eta_0^b$  and  $\eta_3^b = 15/8$ , under the scaling  $\nu_b = \eta_1^b \eta_2^b \eta_3^b$ .

## V. CONCLUSIONS

In conclusion, we investigated the diffraction spectra of FL's in the general case  $\eta = S/(L - S) \neq \tau$ . We have

shown that it is possible to group different Fibonacci lattices into equivalence classes whose elements share the main structural and dynamical properties as witnessed by their diffraction spectra and the energy gaps. These results show that the concept of equivalence classes for FLs has not only a geometrical meaning but also an important role in the scattering, dynamical and thermodynamical properties of the system, contained in the energy spectrum. It is worth stressing once again that this is a consequence of the self-similarity of FSs under the composition rule and that FLs belonging to different equivalence classes cannot be rescaled one over the other. The generator of a class is, in this sense, the simplest structure giving a diffraction pattern which contains the main features common to all of the other elements of the class. Although we focused on the Fibonacci lattices, our arguments apply to the more general class of quasicrystals for which deflation or inflation rules can map the initial lattices into a similar ones.

## Acknowledgments

NL and LD acknowledge financial support from MIUR, through FIRB Project No. RBFR12NLNA\_002. LV and MB acknowledge financial support from Universit degli studi di Padova through *Chip & CIOP* project No. CPDA120359. The authors are thankful to Prof. Camilla Ferrante and Dr. Nicola Rossetto, from the Dipartimento di Chimica, Universit di Padova, for providing access to the direct laser writing setup. The authors thank J. Settino for providing the energy spectra of a particle in a Fibonacci like lattice.

## Appendix A: Generalized Fibonacci lattices from cut and project method

The Fibonacci lattices we considered in the main text can be constructed by means of the cut and project technique. One possible construction has been presented in ref.[21] We prefer to resort to a more standard one and in what follows we will generalize the one given in ref. [3].

Let us introduce a two-dimensional periodic lattice  $\mathcal{I}_2^p$  and its lattice vectors  $\mathbf{e}_1$  and  $\mathbf{e}_2$  such that any point of the lattice can be written as  $\mathbf{p} = n_1 \mathbf{e}_1 + n_2 \mathbf{e}_2$  with  $n_1, n_2 \in \mathbb{Z}$ . Furthermore we introduce the line  $l_\tau$  whose unit vector is  $\hat{l}_\tau = (\cos(\theta_\tau), \sin(\theta_\tau))$  and the unit vector orthogonal to it  $\hat{l}_\tau^\perp = (\sin(\theta_\tau), -\cos(\theta_\tau))$  such that  $\tan(\theta_\tau) = \tau^{-1}$  where  $\tau = (1 + \sqrt{5})/2$ . The canonical Fibonacci lattice is constructed by projecting on the line  $l_\tau$  the points of a square lattice ( $\mathbf{e}_1 \cdot \mathbf{e}_2 = 0$ ,  $|\mathbf{e}_1| = |\mathbf{e}_2|$ ) the points whose Vonroï cell is cut by the line itself. Let us notice that with this procedure the different points are unambiguously numbered on the line  $l_\tau$  once an origin and a direction have been chosen. We are going to construct our Fibonacci lattices using this definition but allowing the two-dimensional lattice to be generic as in Fig.5. Nevertheless we will see that in order to obtain a Fibonacci lattice, namely a one-dimensional set of points whose distances are distributed according to the Fibonacci strings and with the wanted ratio between long and short segments, we

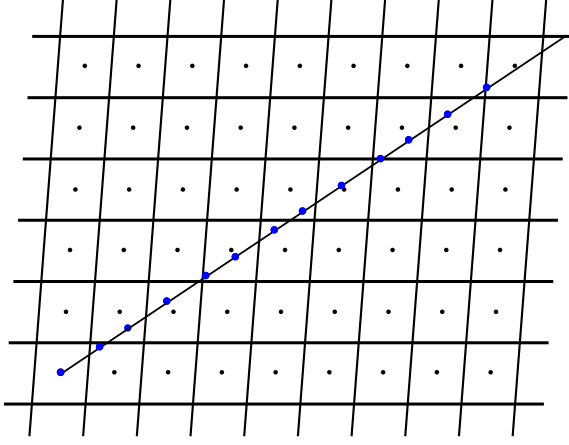


Figure 5: (Color online) Construction of a generalized Fibonacci lattice from a 2D periodic lattice by means of the cut and project method. Blue dots are the projection of points of the 2D lattice whose Voronoi cells are cut by the line  $l_\tau$ .

will have to restrict the set of the allowed two dimensional lattices. Following the discussion in ref.[3] in order for the line  $\gamma \hat{l}_\tau$  to cut the Voronoi cell centered at point  $\mathbf{p}$  it has to intersect the secondary diagonal of the cell (joining the northwest to southeast point of the cell). The diagonals lie on lines parallel to  $\delta(\mathbf{e}_1 - \mathbf{e}_2)$  and whose points are given by  $\delta(\mathbf{e}_1 - \mathbf{e}_2) + n\mathbf{e}_1$  with  $m \in \mathbb{Z}$ . Their intersection with the line  $\gamma \hat{l}_\tau$  occurs at points  $(\frac{n}{\tau}, \frac{n}{\tau^2})$  where  $a = (\tau^2/\sqrt{1+\tau^2})A_{u.c.}/(\mathbf{e}_1 - \mathbf{e}_2) \cdot \hat{l}_\tau^\perp$  and  $A_{u.c.} = (\mathbf{e}_1 \wedge \mathbf{e}_2) \cdot \hat{z}$  is the (oriented) area of the unit cell of the lattice.

This intersection points are inside the Voronoi cell centered at point  $(u, v)$  if and only if

$$u - \frac{|(\mathbf{e}_1 - \mathbf{e}_2) \cdot \hat{x}|}{2} < n a \tau^{-1} < u + \frac{|(\mathbf{e}_1 - \mathbf{e}_2) \cdot \hat{x}|}{2} \quad (\text{A1})$$

$$v - \frac{|(\mathbf{e}_1 - \mathbf{e}_2) \cdot \hat{y}|}{2} < n a \tau^{-2} < v + \frac{|(\mathbf{e}_1 - \mathbf{e}_2) \cdot \hat{y}|}{2} \quad (\text{A2})$$

On the other hand each point of the lattice can be written as  $n_1\mathbf{e}_1 + n_2\mathbf{e}_2$  and  $n_1 + n_2 = n$  because it is the  $n$ -th point to be

projected. Thus we can write  $u = n_1(\mathbf{e}_1 - \mathbf{e}_2) \cdot \hat{x} + n_2 \cdot \hat{x}$  and  $v = n_1(\mathbf{e}_1 - \mathbf{e}_2) \cdot \hat{y} + n_2 \cdot \hat{y}$  and above inequalities become

$$\left(n_1 - \frac{s_x}{2}\right)(\mathbf{e}_1 - \mathbf{e}_2) \cdot \hat{x} < n(a\tau^{-1} - \mathbf{e}_2 \cdot \hat{x}) < \left(n_1 + \frac{s_x}{2}\right)(\mathbf{e}_1 - \mathbf{e}_2) \cdot \hat{x} \quad (\text{A3})$$

$$\left(n_1 - \frac{s_y}{2}\right)(\mathbf{e}_1 - \mathbf{e}_2) \cdot \hat{y} < n(a\tau^{-2} - \mathbf{e}_2 \cdot \hat{y}) < \left(n_1 + \frac{s_y}{2}\right)(\mathbf{e}_1 - \mathbf{e}_2) \cdot \hat{y} \quad (\text{A4})$$

where  $s_x = \text{Sign}((\mathbf{e}_1 - \mathbf{e}_2) \cdot \hat{x})$  and similarly for  $s_y$ . By means of the expression for  $a$  it is easy to prove that  $(a\tau^{-1} - \mathbf{e}_2 \cdot \hat{x})/(\mathbf{e}_1 - \mathbf{e}_2) \cdot \hat{x} = (a\tau^{-2} - \mathbf{e}_2 \cdot \hat{y})/(\mathbf{e}_1 - \mathbf{e}_2) \cdot \hat{y}$  and thus the two inequalities are equivalent to the inequality:

$$\left(n_1 - \frac{1}{2}\right) < \frac{n}{\beta} < \left(n_1 + \frac{1}{2}\right) \quad (\text{A5})$$

$$\beta = 1 - \frac{\mathbf{e}_1 \cdot \hat{l}_\tau^\perp}{\mathbf{e}_2 \cdot \hat{l}_\tau^\perp} = 1 + r \frac{1}{\tau \sin(\alpha) - \cos(\alpha)} \quad (\text{A6})$$

where  $\cos(\alpha) = \mathbf{e}_1 \cdot \mathbf{e}_2 / (|\mathbf{e}_1||\mathbf{e}_2|)$  and  $r = |\mathbf{e}_1|/|\mathbf{e}_2|$ . Being  $n_1$  an integer number the only possibility for the above inequalities to be satisfied is that  $n_1 = \lfloor \frac{n}{\beta} \rfloor$  where  $\lfloor x \rfloor$  is the integer part of  $x$ . After projecting onto  $l_\tau$ , the  $n$ -th point has

coordinates on the the line  $l_\tau$ :

$$x'_n = n \mathbf{e}_2 \cdot \hat{l}_\tau + (\mathbf{e}_1 - \mathbf{e}_2) \cdot \hat{l}_\tau \left\lfloor \frac{n}{\beta} \right\rfloor \quad (\text{A7})$$

By normalizing with respect to  $\mathbf{e}_2 \cdot \hat{l}_\tau$  we eventually obtain the one-dimensional lattice of points

$$x_n = n + \frac{1}{\eta} \left\lfloor \frac{n}{\beta} \right\rfloor \quad (\text{A8})$$

$$\eta^{-1} = \left( \frac{\mathbf{e}_1 \cdot \hat{l}_\tau}{\mathbf{e}_2 \cdot \hat{l}_\tau} - 1 \right). \quad (\text{A9})$$



In order for the above to be a Fibonacci lattice we require  $\beta = \tau$  which is the case for  $\tau r = (\tau \sin(\alpha) - \cos(\alpha))$  and thus  $\eta = (\tau + \tan(\alpha))/((\tau - 1) \tan(\alpha) - \tau^2)$ . Moreover we have to require that  $r > 0$  and  $\eta > 0$  which is the case for  $\tan^{-1}(2\tau + 1) < \alpha < \tan^{-1}(-\tau) + \pi$ . As it can be seen from figs.6 for any given  $\eta > 0$  there correspond a pair  $(r, \alpha)$ :

$$\tan(\alpha) = \tau^2 \frac{\eta\tau + 1}{\eta - \tau} \quad (\text{A10})$$

$$r = \frac{(\tau \tan(\alpha) - 1)}{\tau \sqrt{1 + \tan^2(\alpha)}} \quad (\text{A11})$$

and therefore a two dimensional lattice whose projection on the line  $l_\tau$  returns the wanted FL:

$$x_n^\eta = n - 1 + \frac{1}{\eta} \left\lfloor \frac{n}{\tau} \right\rfloor \quad (\text{A12})$$

$$\eta^{-1} = \left( \frac{\mathbf{e}_1 \cdot \hat{l}_\tau}{\mathbf{e}_2 \cdot \hat{l}_\tau} - 1 \right), \quad (\text{A13})$$

where we shifted the whole lattice in order for the first point to have coordinate  $x_1 = 0$  on the line  $l_\tau$ .

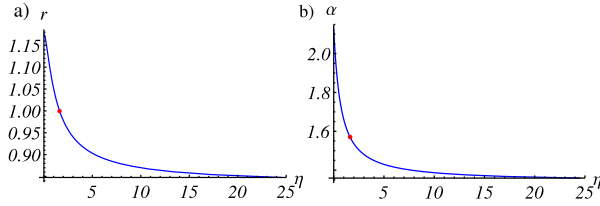


Figure 6: (Color online) **a)** Values of  $r = |\mathbf{e}_1|/|\mathbf{e}_2|$  as a function of  $\eta$ . The red dot corresponds to the point  $(\eta, r) = (\tau, 1)$  for which the canonical Fibonacci lattice is obtained. **b)** Values of the angle  $\alpha$  between  $\mathbf{e}_1$  and  $\mathbf{e}_2$  as a function of  $\eta$ . The red dot corresponds to the point  $(\eta, \alpha) = (\tau, \pi/2)$  for which the canonical Fibonacci lattice is obtained.

## Appendix B: Diffraction pattern

We are interested in the calculation of the quantity:

$$A(q_\parallel) = \lim_{N \rightarrow \infty} \frac{1}{N} \sum_n e^{ix_n^\eta q_\parallel} \quad (\text{B1})$$

where  $x_n^\eta$  are given by eq.A13. Using the unit vectors  $\hat{l}_\tau$  and  $\hat{l}_\tau^\perp$  we can write any point in space as  $\vec{r} = x_\parallel \hat{l}_\tau + x_\perp \hat{l}_\tau^\perp$  and similarly for the variable  $\vec{q} = q_\parallel \hat{l}_\tau + q_\perp \hat{l}_\tau^\perp$ . By introducing the quantity

$$A_X(q_\parallel, q_\perp) = \lim_{N \rightarrow \infty} \frac{1}{N} \sum_n e^{i\vec{p}_n \cdot \vec{q}} \quad (\text{B2})$$

where we recall that  $\vec{p}_n$  are points  $\vec{r}_{n_1 n_2}$  of the two dimensional periodic lattice which lie in a strip of width  $2\Delta =$

$|\mathbf{e}_1 - \mathbf{e}_2| \cdot \hat{l}_\tau^\perp$  around the line  $\gamma \hat{l}_\tau$ . It is easy to see that  $A(q_\parallel) = A_X(q_\parallel, 0)$ . We therefore turn to the calculation of the latter. By introducing the mass density of the two dimensional lattice  $\rho(\vec{r}) = \sum_{m_1 m_2} \delta(\vec{r} - \vec{r}_{m_1 m_2})$  and its Fourier transform  $\rho(\vec{r}) = \int dk_\perp dk_\parallel e^{-i\vec{r} \cdot \vec{k}} \tilde{\rho}(\vec{k})$  we can write:

$$A_X(q_\parallel, q_\perp) = \lim_{L \rightarrow \infty} \frac{1}{L} \frac{1}{2\Delta} \int dk_\perp dk_\parallel \int_{-\Delta}^{\Delta} dx_\perp \int_{-\infty}^{\infty} dx_\parallel e^{i\vec{r} \cdot (\vec{q} - \vec{k})} \tilde{\rho}(\vec{k}) \quad (\text{B3})$$

The above integrals can be calculated:

$$A(q_\parallel) = A_X(q_\parallel, 0) = \int dk_\perp \frac{\sin(k_\perp \Delta)}{k_\perp \Delta} \int dk_\parallel \tilde{\rho}(\vec{k}) \delta(k_\parallel - q_\parallel) \quad (\text{B4})$$

which expresses the fact that the diffraction pattern of an infinite projected quasicrystal is the convolution of the Dirac comb formed by the periodic higher dimensional periodic lattice with the sinc function in the orthogonal space.

In particular  $\tilde{\rho}(\vec{k})$  is a Dirac comb peaked at points  $\mathbf{k}_{hh'} = h\mathbf{w}_1 + h'\mathbf{w}_2$  where we introduced the reciprocal lattice vectors for the dual of the two-dimensional periodic lattice  $\mathcal{I}_2^p$ :

$$\mathbf{w}_1 = \frac{2\pi}{l_1} (\mathbf{e}_1 - \mathbf{e}_1 \cdot \hat{e}_2 \hat{e}_2) \quad (\text{B5})$$

$$\mathbf{w}_2 = \frac{2\pi}{l_2} (\mathbf{e}_2 - \mathbf{e}_2 \cdot \hat{e}_1 \hat{e}_1) \quad (\text{B6})$$

$$(\text{B7})$$

where  $\hat{e}_i = \mathbf{e}_i/|\mathbf{e}_i|$  and  $l_i = |\mathbf{e}_1|^2 - |\mathbf{e}_1 \cdot \hat{e}_2|^2$  and similarly for  $l_2$ . It is easy to check that  $\mathbf{w}_i \cdot \mathbf{e}_j = 2\pi \delta_{ij}$ . In what follows we assume that units are scaled such that  $\mathbf{e}_2 \cdot \hat{l}_\tau = 1$ . In order to evaluate the parallel and perpendicular components of vectors belonging to the reciprocal space we need to evaluate  $\mathbf{w}_i \cdot \hat{l}_\tau$  and  $\mathbf{w}_i \cdot \hat{l}_\tau^\perp$ . In order to do so it is useful to rewrite the vectors  $\mathbf{e}_i$  as linear combinations of  $\hat{l}_\tau$  and  $\hat{l}_\tau^\perp$  by means of the expressions for  $\eta$ ,  $\beta$  and the relation between  $\tan \alpha$  and  $\eta$ . We thus obtain:

$$\mathbf{e}_1 = \left(1 + \frac{1}{\eta}\right) \hat{l}_\tau + \frac{1}{\tau} \left(1 + \frac{1}{\eta}\right) \hat{l}_\tau^\perp \quad (\text{B8})$$

$$\mathbf{e}_2 = \hat{l}_\tau - \left(1 + \frac{1}{\eta}\right) \hat{l}_\tau^\perp \quad (\text{B9})$$

It is now easy to check that:

$$\mathbf{w}_1 \cdot \hat{l}_\tau = \frac{2\pi}{d} \quad \mathbf{w}_2 \cdot \hat{l}_\tau = \frac{2\pi}{\tau d} \quad (\text{B10})$$

$$\mathbf{w}_1 \cdot \hat{l}_\tau^\perp = \frac{2\pi}{d \left(1 + \frac{1}{\eta}\right)} \quad \mathbf{w}_2 \cdot \hat{l}_\tau^\perp = -\frac{2\pi}{d} \quad (\text{B11})$$

where  $d = (\tau + 1/\eta)$ . Therefore we can define:

$$Q(h, h') = \mathbf{k}_{hh'} \cdot \hat{l}_\tau = \frac{2\pi}{d} \left(h + \frac{h'}{\tau}\right) \quad (\text{B12})$$

$$Q_\perp(h, h') = \mathbf{k}_{hh'} \cdot \hat{l}_\tau^\perp = \frac{2\pi}{d} \left(\frac{\eta h}{\eta + 1} - h'\right) \quad (\text{B13})$$

By means of eq.B4 we can thus write the intensities of the diffracted points as:

$$I(q_{\parallel}, \eta) = |A(q_{\parallel})|^2 = \sum_{h, h'} \frac{\sin^2(Q_{\perp}(h, h')\Delta)}{(Q_{\perp}(h, h')\Delta)^2} \delta(q_{\parallel} - Q(h, h')) \quad (\text{B14})$$

where  $\Delta = \tau(1 + 1/\eta)/2$  and we introduce the explicit dependence of the intensity on the parameter  $\eta$  which characterizes the FL. As it can be seen, the diffraction spectrum consists of a set of sharp peaks centered on a dense set of reciprocal lattice points, as by choosing the appropriate values of  $h$  and  $h'$ , any  $q$  can be approximated with arbitrary precision. However, not all these peaks have the same intensity.

In fig.7 we plot  $I(q_{\parallel})$  as given by expression in eq.B14 and its expression calculated explicitly by its definition eq.B1 for a lattice of  $N = 300$  points and  $\eta = 17/6$ . We can see that as expected the peaks' intensities are well captured by eq.B14 even for finite systems especially for peaks characterized by a significant intensity ( $> 0.2$ ).

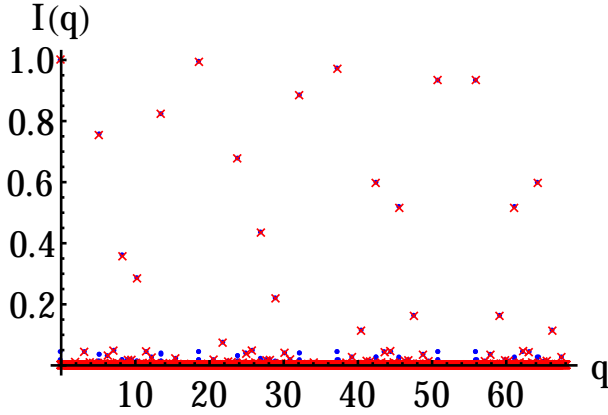


Figure 7: (Color online) Comparison between the values of  $I(q_{\parallel})$  using the cut and project method and the direct evaluation in eq.B1 for a lattice of  $N = 300$  points and  $\eta = 17/6$ . Blue dots are points corresponding to the value in eq.B14 whereas red cross are given by eq.B1.

We now consider the (Fraunhofer) diffraction pattern of a FL  $x_n^{\eta}$ :

$$I(q, \eta) = \lim_{N \rightarrow \infty} \frac{1}{N^2} \left| \sum_n e^{ix_n^{\eta} q} \right|^2. \quad (\text{B15})$$

This quantity is important because it gives a direct experimental access to the reciprocal lattice of our structure. We shall see that this quantity is also encountered in the determination of a (pseudo) energy dispersion relation [23]. In the case of FLs the values of  $q$  at which a non-vanishing intensity is expected are given by:

$$Q(h, h') = \frac{2\pi}{d} \left( h + \frac{h'}{\tau} \right), \quad (\text{B16})$$

where  $d = (\tau + 1/\eta)$ . By properly choosing the integers  $h$  and  $h'$ , any real number can be arbitrarily well approximated, showing that the reciprocal lattice of a FL is dense in  $\mathbb{R}$ , contrarily to periodic lattices which exhibit a discrete reciprocal lattice. Moreover it can be shown [3] that the diffraction pattern has *only* pure point support, lacking of a continuous part (according to the classification of positive measures in the Lebesgue classification).

## Appendix C: Brightest peaks

### 1. Condition for brightest peaks

In order to find the set of points in reciprocal space corresponding to a strong diffracted intensity for a FL, the following condition on the argument of the exponential in the expression for the diffraction pattern has to hold:

$$Q_{\perp}(h, h') \approx 0 \quad (\text{C1})$$

which is satisfied for

$$\frac{h}{h'} \approx 1 + \frac{1}{\eta}. \quad (\text{C2})$$

Let us now consider the equivalence class  $[\eta_0]$  and in particular the sequence  $x_n^{\eta_0}$ . We can write  $\eta_0$  in the continued fraction representation:

$$\eta_0 = a_0 + \frac{1}{a_1 + \frac{1}{a_2 + \frac{1}{a_3 + \dots}}} \equiv [a_0, a_1, a_2, a_3, \dots] \quad (\text{C3})$$

For a rational number the sequence of numbers  $a_i$  is finite, namely  $\eta_0 = [a_0, a_1, \dots, a_n]$ . On the other hand, if  $\eta_0$  is irrational, it is possible to find a rational approximation within the wanted error by increasing the number of terms in its continued fraction representation. It is easy to see that  $\eta_1 = 1 + 1/\eta_0 = [1, a_0, a_1, \dots]$  and in general

$$\eta_k = \underbrace{[1, 1, \dots, 1]}_k, a_0, a_1, \dots]. \quad (\text{C4})$$

With this notation is straightforward to see that regardless of the value of the generator  $\eta_0$ , the sequences of an equivalence class will tend to a Fibonacci sequence since  $\lim_{k \rightarrow \infty} \eta_k = [1, 1, 1, 1, \dots] = \tau$  [24]. Using the continued fraction notation we can write a sequence of rational approximants to  $\eta_0$  as  $a_0, \frac{a_1 a_0 + 1}{a_1}, \frac{a_2(a_1 a_0 + 1) + a_0}{a_2 a_1 + 1}, \dots$ . Since both  $h$  and  $h'$  have to be integers the above condition C2 is satisfied if we choose  $h = s_n + t_n$  and  $h' = s_n$  where  $s_n$  and  $t_n$  are the  $n$ -th approximants of  $\eta_0$  namely  $\eta_0 \approx s_n/t_n$  and can easily be derived from the continued fraction representation of  $\eta_0$ .

It is worth stressing that if  $\eta_0$  is a rational number ( $\eta_0 = a/b$ , with  $a, b \in \mathbb{N}$ )  $h$  and  $h'$  can be chosen such that  $h/h' = (a + b)/a$ . Thus, at points  $q_m = Q(m(a + b), mb) = 2m\pi$  ( $m \in \mathbb{Z}$ ) we have that  $I(q_m, \eta_0) = 1$ . On the other hand, for irrational  $\eta_0$  the condition is never satisfied exactly but we can resort to the rational approximants of  $\eta_0$  to estimate the positions at which the brightest peaks appear.

## 2. Relation between positions of brightest peaks

Let  $x_n^{\eta_0}$  and  $x_n^{\eta_1}$  be two Fibonacci lattices belonging to the same equivalence class and their associated reciprocal lattices  $Q_0(h, h') = 2\pi d_0^{-1}(h + h'/\tau)$ ,  $Q_1(h, h') = 2\pi d_1^{-1}(h + h'/\tau)$  respectively, where  $d_i = \tau + 1/\eta_i$ . By defining  $h_n$  ( $k_n$ ) and  $h'_n$  ( $k'_n$ ) as the numerator and denominator of the  $n$ -th rational approximants of  $1 + 1/\eta_0$  ( $1 + 1/\eta_1$ ), the following relations hold true  $k_n = h_n + h'_n$  and  $k'_n = h_n$ . By inserting these relations into the expression for  $Q_1(k, k')$  we get:

$$\begin{aligned} Q_1(k_n, k'_n) &= \frac{2\pi}{d_1} \left( k_n + \frac{k'_n}{\tau} \right) = \frac{2\pi}{d_1} \left( h_n + h'_n + \frac{h_n}{\tau} \right) \\ &= \frac{2\pi\tau}{d_1} \left( h_n + \frac{h'_n}{\tau} \right) = \frac{d_0\tau}{d_1} \frac{2\pi}{d_0} \left( h_n + \frac{h'_n}{\tau} \right) \\ &= \frac{d_0\tau}{d_1} Q_0(h_n, h'_n) = \eta_1 Q_0(h_n, h'_n) \end{aligned}$$

where in the last line we used the fact that  $d_0\tau/d_1 = \eta_1$ . This means that the lattice obtained by applying the composition rule  $\mathcal{C}(x_n^{\eta_0}) = \eta_1 x_n^{\eta_1}$  has brightest peaks at the same positions of the original lattice only rescaled by a factor  $\eta_1$ .

## 3. Relation between intensities of brightest peaks

From eq.B14 we can also estimate the relation between the intensities of the brightest peaks in the diffraction spectrum of two FL belonging to the same class. Using the expression in eq.B14 and assuming  $k_\perp \Delta \approx 0$  we can write  $\sin^2(k_\perp \Delta)/(k_\perp \Delta)^2 - 1 \approx (k_\perp \Delta)^2/9$ . Using the condition for  $k_\perp \approx 0$  and following a calculation similar to that to determined relation between the positions of the brightest peaks we find that  $(k_\perp^1 \Delta_1)^2 = (k_\perp^0 \Delta_0)^2/\tau^2$ . Therefore we have

$$I(\eta_1 q, \eta_1) \approx I(q, \eta_0) + \frac{1}{\tau}(1 - I(q, \eta_0)), \quad (\text{C5})$$

meaning that the intensities of brightest peaks of the scaled lattice are more intense of those of the original lattice by a term proportional to the difference between the maximum attainable intensity and the intensity of the original lattice intensities.

In fig.8 we plot the quantities (blue dots)  $\tau^{-1}(1 - I(q, \eta_0))$  and (red cross)  $(I(\eta_1 q, \eta_1) - I(q, \eta_0))$  for  $q$  such that  $I(q, \eta_0) > 0.5$  and for lattices of  $N = 300$  sites and  $\eta_0 = 6/11$  and  $\eta_1 = 1 + 1/\eta_0$  respectively.

## Appendix D: Experimental setup

To test experimentally the diffraction from FL's, a series of quasi-periodic diffraction gratings have been prepared using a photorefractive direct laser writing (DLW) technique [25]. This technique consists in scanning with a focused laser beam a photorefractive sample, engraving on it a series of lines with a modified refractive index with respect to the rest of the sample. The scanning movement is performed by translating the

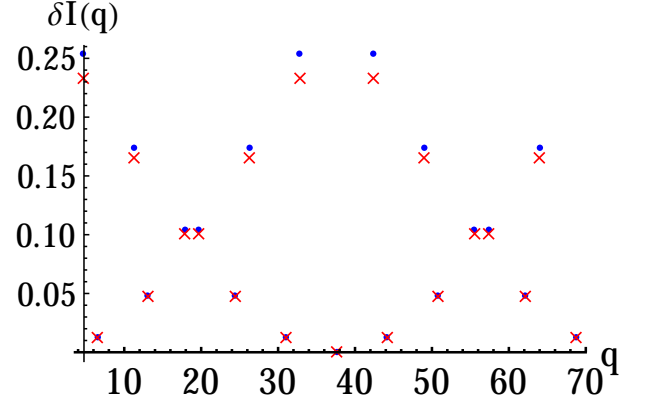


Figure 8: (Color online) Plot of (blue dots)  $\tau^{-1}(1 - I(q, \eta_0))$  and (red cross)  $(I(\eta_1 q, \eta_1) - I(q, \eta_0))$  for those  $q$  for which  $I(q, \eta_0) > 0.5$  showing that the intensities of the brightest peaks of the diffraction pattern of a FL  $x_n^{\eta_1}$  generated from a FL  $x_n^{\eta_0}$  by means of the composition rule are more intense of those of the original lattice by a factor of  $\tau$ .

sample with the aid of a computer-controlled XY stage at constant speed of  $50 \mu\text{m/s}$ . The nominal precision of the translation stage is  $0.5 \mu\text{m}$  for the conditions used in this experiment. A frequency doubled diode pumped Nd:YWO<sub>4</sub> solid state laser (Coherent Verdi V5) emitting a CW beam at 532 nm has been used as light source for DLW. The beam was suitably attenuated by a series of neutral density filters and sent to a focusing microscope objective (Olympus 100X/0.80) so that the power after the objective was set at 17 mW. The substrate used to engrave the optical structures is a slab of photorefractive lithium niobate doped with iron at the nominal concentration of 0.1 mol% in the melt. The sample was X-cut with dimensions (X × Y × Z) 1mm × 8mm × 13mm and the lines were written on the X face, by scanning along the Y direction with an ordinarily polarized beam. This process can induce extraordinary refractive index changes as large as  $10^{-3}$  in the written lines and therefore can be used to produce arbitrary diffraction structures. The diffraction pattern of these structures was measured with the help of a computer-controlled optical diffractometer in which the sample and the detector were mounted on two co-axial goniometers that were independently controlled by a computer [26]. An optical beam produced by a He-Ne laser at 632.8 nm with a power of 4 mW was expanded, polarized along the extraordinary direction and finally transmitted through the sample surface, resulting in a clearly visible diffraction pattern. This pattern was measured by a Si photodiode and a lock-in amplifier and recorded on the computer as a function of the detector and of the sample angle.



## Appendix E: Experimental diffraction patterns

### 1. Structure factor

In order to compare the experimental data with the theoretical calculation we need to take into account that our gratings are made up of a (quasi) periodic repetition of a region with a modified refractive index,  $\Delta n(x)$ . This leads to the fact, well known from standard diffraction theory, that the diffracted intensity in reciprocal space is proportional to the product of two terms: a first one,  $S(q) = \left| \int \Delta n(x) e^{ixq} dx \right|^2$  which depends on the detailed structure of the repeated unit of the grating (*structure factor*) and a second term due to lattice geometry, which is the true object of this study:

$$I_R(q, \eta) = S(q) \frac{1}{N^2} \left| \sum_n e^{ix_n \eta} \right|^2 = S(q) I(q, \eta) \quad (\text{E1})$$

The structure factor modulates the intensity of the lattice diffraction pattern, complicating the comparison between experiments and theory. In principle  $S(q)$  could be calculated by knowing the details of the refractive index profile changes produced by our technique. Here we used another approach which exploits the fact our samples differ only for the line position sequence  $x_n$ . We can use therefore the periodic grating (Fig. 9) to measure the function  $S(q)$  directly at the reciprocal lattice points  $\{q_M^i\}$  of the periodic grating, where  $I(q_M^i)$  has local maxima.

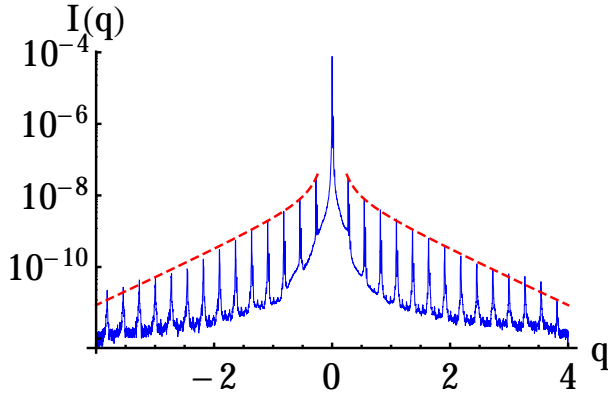


Figure 9: (Color online). Experimental diffraction pattern of the periodic grating with spacing  $L = 23 \mu\text{m}$  (blue, solid curve) and fit of the satellite peak intensities using function E2 (red, dashed curve).

We found that the following phenomenological functional

form for  $S(q)$  describes adequately the peak intensity in the whole range of measured values (see fig. 9):

$$S(q) = S_0 e^{-\lambda q - \frac{q_0}{q}} \quad (\text{E2})$$

where the parameters  $S_0, \lambda, q_0$  are determined by a least square fit in the range  $q \in [0.5, 3] \mu\text{m}^{-1}$  excluding the last peaks because the corresponding momenta where comparable with a length scale of the order of the optical waveguide width. We also notice that all measured diffraction patterns drop almost to zero outside the interval  $q \in [-4, 4] \mu\text{m}^{-1}$ ; this is due to the fact that our lines have a width determined by the laser writing optics which is not smaller than  $2 \mu\text{m}$ , so that our diffraction pattern cannot probe  $|q| > 3 \mu\text{m}^{-1}$ .

### 2. Comparison with theoretical patterns

In Fig. 10 we compare the theoretical diffraction pattern  $I(q, \eta)$  with the experimental data points for the grating  $\eta_3^b$ . The intensity of the experimental points has been rescaled to take into account the contribution of the structure factor of the grating and the  $q$  axis of the experimental plot has been rescaled in order to compare it with the simulation, which considers FL's with  $S = 1$ . A similar figure is obtained for the case  $\eta_1^a = 17/6$ . The agreement is very satisfactory: not only the position but also the intensity of the diffraction peaks are correctly obtained, confirming that our approach is reliable.

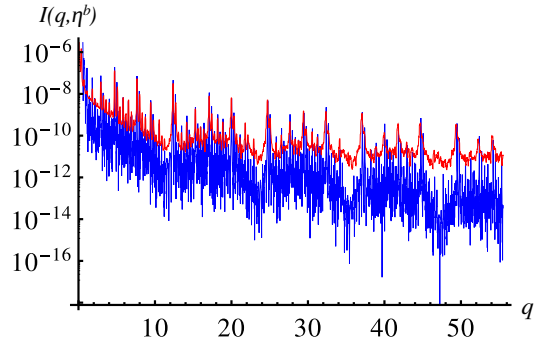


Figure 10: (Color online). Experimental diffraction pattern (solid red top curve) compared with the theoretical diffraction pattern with the inclusion of the structure factor (solid blue bottom curve) for a Fibonacci grating with  $N = 300$  lines and  $L = 23 \mu\text{m}$  and  $S = 15 \mu\text{m}$ ,  $\eta_3^b = 1.875$ .

[1] D. Shechtman, I. Blech, D. Gratias, and J. W. Cahn, Phys. Rev. Lett. **53**, 1951 (1984).  
 [2] D. Levine, and P.J. Steinhardt, Phys. Rev. B **34**, 596 (1986).  
 [3] M. Senechal, *Quasicrystals and geometry*, Cambridge University Press (1995).

[4] C. Janot, *Quasicrystals - A primer* (second edition), Oxford University Press (1994).  
 [5] Y. E. Kraus, and O. Zilberberg, Phys. Rev. Lett. **109**, 116404 (2012).  
 [6] Y. E. Kraus, Y. Lahini, Z. Ringel, M. Verbin, and O. Zilberberg,

- Phys. Rev. Lett. **109**, 106402 (2012).
- [7] M. Verbin, O. Zilberberg, Y. E. Kraus, Y. Lahini, and Y. Silberberg, Phys. Rev. Lett. **110**, 076403 (2013).
  - [8] M. Lohse, C. Schweizer, O. Zilberberg, M. Aidelsburger, and I. Bloch, Nat. Phys. **3584** (2015).
  - [9] K. Singh, K. Saha, S. A. Parameswaran, and D. M. Weld, Phys. Rev. A **92**, 063426 (2015).
  - [10] R. W. Peng, Y. M. Liu, X. Q. Huang, F. Qiu, Mu Wang, A. Hu, S. S. Jiang, D. Feng, L. Z. Ouyang, and J. Zou, Phys. Rev. B **69**, 165109 (2004).
  - [11] A. Lin, Y. K. Zhong, S. M. Fu, C. W. Tseng, and S. L. Yan, Opt. Expr. **22** (53) a880 (2014).
  - [12] A. Gopinath, S. V. Boriskina, N. - N. Feng, B. M. Reinhard, and L. Dal Negro, Nano Lett. **8**, 2423 (2008).
  - [13] X. Huang, and M. L. Brongersma, Nano Lett., **13**, 5420 (2013).
  - [14] Y. W. Lee, F. C. Fan, Y. C. Huang, B. Y. Gu, B. Z. Dong, and M. H. Chou, Opt. Lett. **27**, 2191 (2002).
  - [15] P. Y. Chou, W. K. Chang, H. P. Chung, and Y. H. Chen Opt. Express, **22** (23) 28857 (2014).
  - [16] N. D. Lanzillotti-Kimura, A. Fainstein, B. Jusserand, A. Lemaitre, O. Mauguin, and L. Largeau, Phys. Rev. B **76**, 174301 (2007).
  - [17] A. R. Overy, A. B. Cairns, M. J. Cliffe, M. G. Tucker, and A. L. Goodwin, arXiv:1508.05909.
  - [18] Ch. Li, H. Cheng, R. Chen, Tian. Ma, Li-G. Wang, Yu. Song, and Hai-Q. Lin, Appl. Phys. Lett. **103**, 172106 (2013).
  - [19] L. Dal Negro (ed.) Optics of Aperiodic Structures: Fundamentals and Device Applications, Pan Stanford University Publishing (2014).
  - [20] G. Radons, W. Just and P. Hussler (eds.) *Collective Dynamics of Nonlinear and Disordered Systems*, Springer - Verlag, Berlin - Heidelberg (2005).
  - [21] P. Buczek, L. Sadun, and J. Wolny, Acta Physica Polonica B, **36**, 3 (2005).
  - [22] J.-M. Luck Phys. Rev. B **39**, 5834 (1989).
  - [23] J.-M. Gambaudo, and P. Vignolo, New J. Phys. **16**, 043013 (2014).
  - [24] This can also be seen by explicit calculation, in fact it is possible to show that  $\eta_k = \frac{F_{k+1}\eta_0 + F_k}{F_k\eta_0 + F_{k-1}}$ , where  $F_k$  are the Fibonacci numbers ( $F_0 = 0$ ). The above expression tends to  $\tau$  as  $k \rightarrow \infty$  due to the fact that  $F_{k+1}/F_k \rightarrow \tau$  in this limit.
  - [25] L. Vittadello, A. Zaltron, N. Argiolas, M. Bazzan, N. Rossetto, and R. Signorini, J. Phys. D **49**, 125103 (2015).
  - [26] M. Bazzan, N. Argiolas, C. Sada, P. Mazzoldi, S. Grilli, P. Ferraro, P. De Natale, and L. Sansone, Ferroelectrics **352**, 25 (2007).